Avalanche-Induced Current Enhancement in Semiconducting Carbon Nanotubes

Albert Liao,[1] Yang Zhao,[1] and Eric Pop[1,2,*]

[1]Department of Electrical and Computer Engineering, Micro and Nanotechnology Laboratory, University of Illinois, Urbana-Champaign, Illinois 61801, USA

[2]Beckman Institute, University of Illinois, Urbana-Champaign, Illinois 61801, USA

(Received 8 August 2008; published 16 December 2008)

Semiconducting single-wall carbon nanotubes under high electric field stress (~10 V/μm) display a remarkable current increase due to avalanche generation of free electrons and holes. Unlike other materials, the avalanche process in such 1D quantum wires involves access to the third subband and is insensitive to temperature but strongly dependent on diameter $\sim \exp(-1/d^2)$. Comparison with a theoretical model yields a novel approach to obtain the inelastic optical phonon emission length $\lambda_{\mathrm{OP,ems}} \approx 15d$ nm. The new results underscore the importance of multiband transport in 1D molecular wires.

DOI: 10.1103/PhysRevLett.101.256804 PACS numbers: 73.63.Fg, 72.10.−d, 73.22.−f, 73.23.−b

Electrical transport in one-dimensional (1D) nanomaterials is of much fundamental and practical interest. Among these, single-wall carbon nanotubes have remarkably high performance, displaying quasiballistic transport at submicron lengths [1], and excellent low-field mobility even in longer, diffusive samples [2]. Despite such progress, less is known about diffusive transport at high fields (>1 V/μm). This regime sets the peak current-carrying ability and provides a glimpse into the behavior under extreme electrical stress conditions. For instance, the maximum current of long *metallic* single-wall nanotubes (m-SWNTs) is 20–25 μA when limited by Joule heating and optical phonon scattering [3,4], which appears to be exceeded only in submicron, quasiballistic samples [1]. The maximum current capacity of long *semiconducting* single-wall nanotubes (s-SWNTs) under diffusive transport is less established, although a 25 μA limit has been suggested for single-band conduction [5]. However, experimental data indicate that this limit is exceeded under ambipolar transport [6], and theoretical estimates suggest that this value can be surpassed when multiple subbands are involved [7].

In this Letter, we report a remarkable current increase beyond the 25 μA "diffusive limit" in Ohmically contacted s-SWNTs under avalanche impact ionization conditions. We investigate transport up to electrical breakdown and find the current in s-SWNTs first plateaus near ~25 μA and then sharply increases at high fields (~10 V/μm). This behavior is not seen in the many m-SWNTs tested. The current "up-kick" is attributed to the onset of avalanche impact ionization (II), a phenomenon observed in semiconductor $p-n$ diodes and transistors at high fields [8–11] but not previously measured in nanotubes. We explore the behavior of s-SWNTs in avalanche conditions and demonstrate a novel approach for obtaining the optical phonon (OP) scattering length, which is the strongest energy relaxation process at high fields and itself a fundamental transport parameter.

Carbon nanotubes were grown by chemical vapor deposition from a patterned Fe catalyst on 100 nm thermal SiO_2 and highly p-doped Si wafers which also serve as back gates. The nanotubes were contacted by evaporating 40 nm of Pd, as shown in Figs. 1(a) and 1(b). Electrode separation varied from $L \sim 1$–4 μm, and typical contact resistance was Ohmic, $R_C \sim 30$–50 kΩ estimated from the low-field $I_D - V_{\mathrm{DS}}$ slope at high V_{GS}. Metallic and semiconducting nanotubes were sorted by their on/off ratios, measuring current (I_D) vs gate-source voltage (V_{GS}), as in Fig. 1(c). As-grown devices show unipolar p-type behavior with negative threshold voltage (V_T). Dimensions were obtained by atomic force microscopy (AFM), indicating diameters in the range $d \sim 2$–3.6 nm.

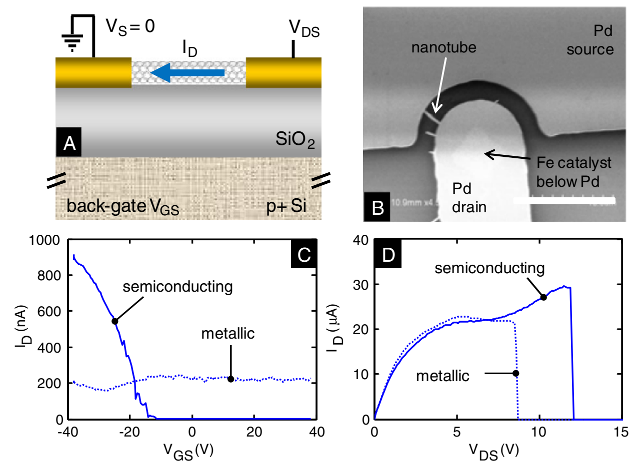

FIG. 1 (color online). (a) Schematic cross section of a back-gated nanotube. (b) Scanning electron microscope top-view image of a fabricated device. Semicircular electrodes are used for tighter control of the device length. The scale bar is 10 μm. (c) Back-gate voltage dependence (V_{GS}) of semiconducting and metallic SWNTs showing typical on/off ratios. (d) Drain voltage (V_{DS}) dependence up to breakdown in air of semiconducting and metallic SWNTs. The metallic device saturates before breakdown, but the semiconducting one displays an up-kick in current. Compared devices have similar diameter $d \sim 2.5$ nm and length $L \sim 0.8$–1.1 μm.

 © 2008 The American Physical Society

Current vs drain-source voltage (V_{DS}) measurements were made in air and vacuum. In air, m-SWNTs saturate from self-heating and strong electron-phonon scattering [4] up to Joule breakdown. By contrast, most s-SWNTs exhibit a sharp current increase before Joule breakdown [comparison in Fig. 1(d)]. Additional measurements in vacuum ($\sim 10^{-5}$ Torr, Figs. 3 and 4) allow further study of the current up-kick without breaking the nanotubes by oxidation. It is important to note that devices were measured in the reverse bias regime, with $V_{GS} < 0 < V_{DS}$ and $|V_{GS}| > |V_{DS}|$ [7]. By contrast, in Schottky midgap contacted devices, the ambipolar regime $V_{DS} < V_{GS} < 0$ "splits" the potential drop along the channel, resulting in lower longitudinal electric fields [6,7,12] and transport by both electrons and holes. In the reverse bias regime, holes are the majority carriers in our s-SWNTs until the avalanche mechanism partially turns on the conduction band [Fig. 2(a)].

At first glance, several mechanisms may be responsible for the current increase at very high fields in our s-SWNTs, all various forms of "soft" (reversible) breakdown [13]. These are Zener band-to-band (BB) tunneling, avalanche II, and thermal generation current. Under BB transport, electrons tunnel from the valence to the conduction band. The probability is evaluated as $P_{BB} \sim \exp(-E_G^2/q\hbar v_F F)$, where E_G is the band gap ($\sim 0.84/d$ eV, where d is in nanometers), v_F is the Fermi velocity, and F is the electric field [14]. During avalanche II, holes gain high energy in the valence band and then lose it by creating electron-hole pairs (EHPs) as shown in Fig. 2(a). Inelastic OP emission is the strongest process competing with II, given the large OP energy ($\hbar\omega_{OP} \sim 0.18$ eV). The II probability is estimated as $P_{II} \sim \exp(-E_{TH}/q\lambda_{OP,ems}F)$ [8,15,16]. We first take $\lambda_{OP,ems} \sim 14d$ nm as the spontaneous OP emission mean free path (MFP) by holes or electrons [16], and E_{TH} is the avalanche energy threshold. Comparing the two mechanisms in Fig. 2(b) suggests that impact ionization is considerably more likely for the electric field and nanotube diameter range in this study. BB transport becomes important as a result of sudden spatial changes in electrostatic or chemical doping, leading to local fields of the order 100 V/μm (1 MV/cm) or higher [17,18]. Thermal generation is experimentally investigated in Fig. 3(c) and also found to have a negligible contribution, as explored in more detail below.

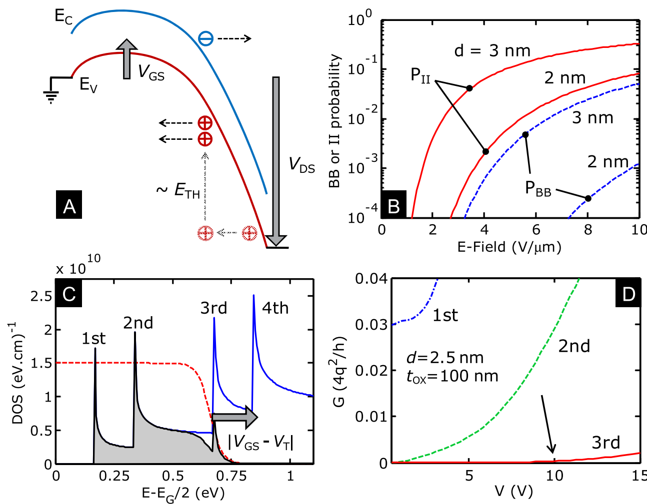

FIG. 2 (color online). Theoretical basis for avalanche behavior of s-SWNTs. (a) Schematic band diagram and EHP generation under reverse bias. (b) Probability of II and Zener BB tunneling vs electric field along the nanotube, for the diameters and field range of interest. (c) Computed DOS showing the first four subbands. The second band begins to fill at $|V_{GS} - V_T| \sim 5$ V and the third at $|V_{GS} - V_T| \sim 15$ V, as pictured. (d) Contact conductance of the first three subbands under direct injection from the Pd electrode. The arrow indicates approximate voltage at which direct injection into the third subband becomes significant. Plots (c) and (d) were obtained for $d = 2.5$ nm and $t_{ox} = 100$ nm.

Previous theoretical work has shown II in s-SWNTs is not possible until the third subband is occupied [16], due to angular momentum conservation. Hence, the II threshold energy measured from the edge of the first band scales as $E_{TH} \sim 3/2E_G \sim 1.26/d$ eV, which is greater than the band gap, as is typical in other semiconductors [10,11]. To determine if the third subband is populated in our experiments, we look at the nanotube density of states (DOS), in Fig. 2(c). Each van Hove singularity represents the beginning of a subband. As V_{GS} is lowered beyond threshold, the Fermi level inside the nanotube shifts to the right on the DOS plot, and the third subband begins to fill at approximately $|V_{GS} - V_T| \sim 15$ V. The observed V_T for our devices is in the range of -7 to -15 V. Thus, filling the third subband is within reach experimentally, as an avalanche is seen at various V_{GS} in Fig. 3. In addition, we find that direct injection into higher subbands at the contacts is also possible, as previously suggested [7]. We estimate this in Fig. 2(d) using a WKB integral to calculate the conductance associated with direct injection into the first three subbands at the Pd electrode. Naturally, injection into higher subbands depends strongly on voltage, and, while direct injection into the third band is possible, we expect that high-field intervalley scattering [19,20] and gate-controlled charge distribution [Fig. 2(c)] are primarily responsible for populating the higher subbands.

The effects of gate voltage, nanotube length, and temperature on the avalanche current are shown in Fig. 3. First, for a given length, a similar current up-kick is observed at high lateral fields at any gate voltage V_{GS} beyond threshold. In other words, the four data curves converge on the up-kick region at high lateral drain voltage V_{DS} in Figs. 3(a) and 3(b). Second, for a similar diameter (similar band separations and II threshold E_{TH}), the onset of the avalanche up-kick is seen around the same approximate *field* ($\sim V_{DS}/L$), not the same drain voltage. The two data sets in Figs. 3(a) and 3(b) suggest that filling the third subband at large gate voltage is a necessary, but not sufficient, condition to induce current enhancement through

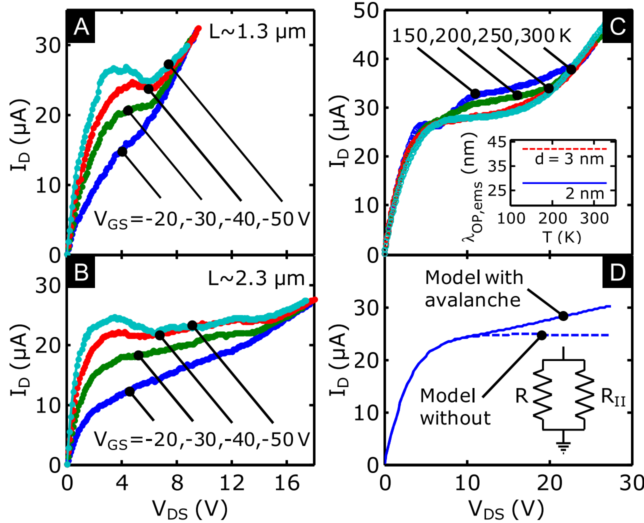

FIG. 3 (color online). Length and temperature dependence of impact ionization. (a),(b) Measured reverse bias current vs drain voltage (V_{DS}) in vacuum with various V_{GS} for s-SWNTs of similar diameter ($d \sim 2.5$ nm) but different lengths: (a) $L \approx 1.3$ μm and (b) $L \approx 2.3$ μm. The onset for the avalanche up-kick scales as the lateral *field* and appears independent of V_{GS}. (c) Measured reverse bias $I_D - V_{DS}$ for s-SWNTs with $d \sim 2.2$ nm and $L \approx 2.2$ μm, in vacuum. There is little temperature dependence of the avalanche behavior, attributed to the temperature insensitivity of the optical phonon emission mean free path ($\lambda_{OP,ems}$ calculated for two diameters in the inset). (d) Model including and excluding impact ionization as a second parallel channel which begins to open up at high field [see text and also Figs. 1(d) and 2(a)].

hole avalanche. A high lateral electric field set by the drain voltage is also required to create the signature up-kick in the measured *I*-*V* characteristics.

An important feature of the avalanche process in many semiconductors such as silicon is the negative temperature dependence of the II coefficient [9]. As the phonon scattering rate increases with temperature, free carriers gain less energy from the field and the II rate decreases at higher temperatures. Here such trends are examined in Fig. 3(c), showing experimental data taken from 150 to 300 K. Unlike in silicon, we observe negligible temperature dependence of the high-bias impact ionization region. The essential difference lies in that the OP emission MFP ($\lambda_{OP,ems}$) varies minimally with temperature in SWNTs. As the OP energy is much greater than in other materials, the OP occupation $N_{OP} = 1/[\exp(\hbar\omega_{OP}/k_B T) - 1]$ is very small ($\ll 1$), where k_B is the Boltzmann constant. Following Ref. [4], the spontaneous OP emission MFP can be written as $\lambda_{OP,ems} = [N_{OP}(300) + 1]/[N_{OP}(T) + 1]\lambda_{OP,300}$, where $\lambda_{OP,300} \approx 14d$ [16]. This MFP is shown for two diameters as the inset in Fig. 3(c), illustrating the negligible temperature variation. The lack of temperature dependence and that of a notable current dependence (Joule heating) of the up-kick also indicate that there is no significant contribution from thermal current generation. Quite the opposite, given the generation of EHPs rather than OPs during II, a lowered Joule heating rate in the highest field region near the drain is expected.

In order to better understand the field dependence of the avalanche process, we have modified an existing SWNT model [4] by including II as an additional current path through a parallel resistor. The choice is motivated by the physical picture in Fig. 2(a), which shows electron transport in the conduction band "turning on" as an additional channel at fields high enough to induce hole-driven II. The expression for this resistor is given as $R_{II} = R\exp(E_{TH}/q\lambda_{OP,ems}F)$, where R is for single-band transport, computed self-consistently with the SWNT temperature [4]. The results are shown in Fig. 3(d) with $\lambda_{OP,ems}$ included as mentioned above and without any other adjustable parameters. Despite being an "augmented" single-band model, the simulation correctly captures the experimentally observed current up-kick and its delayed voltage onset [also see Fig. 1(d)]. The simple analysis also allows us to gain physical insight into the avalanche process and to intuitively extract a few more key parameters.

In the parallel resistor approach, the avalanche current is $I_{II} \approx I_S \exp(-E_{TH}/q\lambda_{OP,ems}F)$, where I_S is the saturation current reached before II becomes significant. Inserting the expected diameter dependence $E_{TH} \approx E_1/d$ and $\lambda_{OP,ems} \approx \lambda_1 d$, we obtain $I_{II} \approx I_S \exp(-E_1/q\lambda_1 F d^2)$, where E_1 and λ_1 are the threshold energy and MFP for a nanotube of diameter 1 nm. Consequently, the average field at which $I_{II} = I_S/2$ is given by $\langle F_{TH}\rangle \approx E_1/q\lambda_1 d^2 \ln(2)$. The experimental data in Fig. 4(a) can be used to extract this field (but not the peak field) in our devices, which is plotted vs $1/d^2$ for nanotubes of several diameters ($d \sim 2.2$–3.6 nm) in Fig. 4(b). The slope of the linear fit thus scales as the ratio between the II threshold energy and the inelastic MFP E_1/λ_1. However, the avalanche process is a strong function of the field, and most EHPs are generated at the peak field $F_{TH,MAX}$. The latter is estimated by noting that the potential near the drain has a dependence $V(x) \approx \ell F_0 \sinh(x/\ell)$, where $F_0 \sim 1$ V/μm is the saturation velocity field [6] and ℓ is an electrostatic length scale comparable to t_{ox} [21,22]. Fitting this expression to our voltage conditions and nanotube dimensions, we find $F_{TH,MAX}/\langle F_{TH}\rangle \approx 4.5$ for a $L = 1$ μm device and 3.5 for $L = 2$ μm. Thus, using the peak instead of the average field, the empirically extracted slope gives $E_1/\lambda_1 \sim 0.088$ eV nm, where we take $E_1 = 1.26$ eV as the bottom of the third subband. Accounting for fit errors, this yields $\lambda_1 = 15 \pm 3$ nm as the inelastic OP emission MFP for $d = 1$ nm, or generally $\lambda_{OP,ems} = \lambda_1 d$. This value is in good agreement with the theoretically predicted $14d$ nm in Ref. [16], and our approach demonstrates a novel empirical method for extracting this important transport parameter from high-field electrical measurements.

Before concluding, it is interesting to compare our results to those of Marty *et al.* [23], who studied exciton formation during high-field unipolar transport in SWNTs.

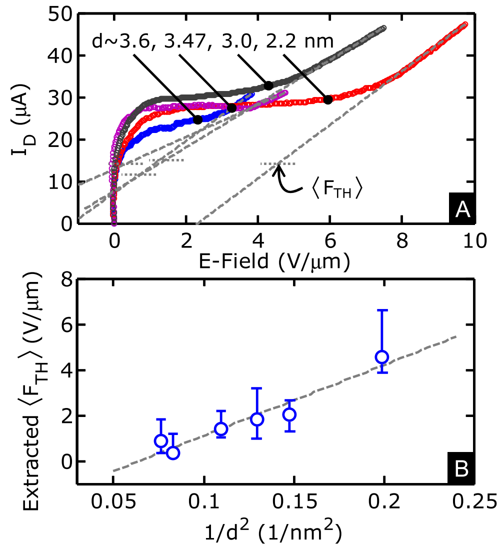

FIG. 4 (color online). Diameter dependence of avalanche threshold field F_{TH}. (a) Current vs average channel field $(V_{\mathrm{DS}} - I_D R_C)/L$ for several diameters, and lengths between 2.2–4.1 μm. The II threshold is extrapolated from the tail region and defined as the field $\langle F_{\mathrm{TH}} \rangle$ at which the current reaches half the saturation value. (b) Extracted $\langle F_{\mathrm{TH}} \rangle$ vs $1/d^2$. The uncertainty in diameter from AFM measurements is 0.4 nm. The slope of the linear fit scales as the ratio between the avalanche energy threshold and the inelastic OP emission length $E_{\mathrm{TH}}/\lambda_{\mathrm{OP,ems}}$. Taking $E_{\mathrm{TH}} \sim 1.26/d$ eV, the OP emission length is $\sim 15d$ nm.

They observed radiative exciton recombination at high fields but did not observe the dramatic current increase before breakdown. This was reasonably attributed to direct exciton annihilation rather than the avalanche generation of free carriers. By contrast, our nanotubes have $\sim 2\times$ larger diameters and thus approximately half the band separations and exciton binding energies, and Ohmic Pd contacts rather than Schottky Co contacts. In addition, all of our measurements except Fig. 1(d) were made in vacuum, allowing repeated study of the current up-kick, which was not always observable in air before Joule breakdown [24]. While excitonic generation and recombination may play a role in our samples, we suggest that the current increase is possible because most free EHPs are generated in the high-field region within a few mean free paths (10–100 nm) of the drain. Thus, generated electrons are swept out into the electrode by the high field within 0.1–1 ps [Fig. 2(a)], much faster than the recombination lifetimes (10–100 ps) [26]. In addition, the high temperatures and high fields in these conditions contribute significantly to exciton instability, despite their relatively high binding energy.

In summary, we observe a remarkable current increase in 1–4 μm long semiconducting SWNTs driven into avalanche impact ionization at high field ($\sim$10 V/μm). Analyzing near-breakdown I-V data, we find that the avalanche process is nearly temperature-independent but strongly diameter-dependent $\sim \exp(-1/d^2)$, unlike in other materials. In addition, a novel estimate of the inelastic OP emission length $\lambda_{\mathrm{OP,ems}} \approx 15d$ nm is obtained by fitting against a model of the avalanche current. We note that upper subband transport must be considered at high bias and has a significant effect on the current-carrying capacity of such nanomaterials. The results also suggest that avalanche-driven devices with highly nonlinear characteristics can be fashioned from s-SWNTs.

We acknowledge valuable discussions with D. Jena, M. Kuroda, J.-P. Leburton, and M. Shim. This work was supported in part by the University of Illinois, the NSF NCN, and the Nanoelectronics Research Initiative (NRI) MIND center.

*epop@illinois.edu

[1] A. Javey *et al.*, Phys. Rev. Lett. **92**, 106804 (2004).
[2] X. J. Zhou *et al.*, Phys. Rev. Lett. **95**, 146805 (2005).
[3] Z. Yao, C. L. Kane, and C. Dekker, Phys. Rev. Lett. **84**, 2941 (2000).
[4] E. Pop *et al.*, J. Appl. Phys. **101**, 093710 (2007).
[5] D. Jena, arXiv:0804.3997.
[6] Y. F. Chen and M. S. Fuhrer, Phys. Rev. Lett. **95**, 236803 (2005).
[7] Y. Ouyang, Y. Yoon, and J. Guo, J. Comput.-Aided Mater. Des. **14**, 73 (2007).
[8] F.-C. Hsu *et al.*, IEEE Trans. Electron Devices **29**, 1702 (1982).
[9] C. R. Crowell and S. M. Sze, Appl. Phys. Lett. **9**, 242 (1966).
[10] C. L. Anderson and C. R. Crowell, Phys. Rev. B **5**, 2267 (1972).
[11] J. Allam, Jpn. J. Appl. Phys. **36**, 1529 (1997).
[12] J. Tersoff *et al.*, Appl. Phys. Lett. **86**, 263108 (2005).
[13] E. A. Amerasekera and C. Duvvury, *ESD in Silicon Integrated Circuits* (Wiley, New York, 2002).
[14] K. Bosnick, N. Gabor, and P. McEuen, Appl. Phys. Lett. **89**, 163121 (2006).
[15] W. Shockley, Solid-State Electron. **2**, 35 (1961).
[16] V. Perebeinos and P. Avouris, Phys. Rev. B **74**, 121410(R) (2006).
[17] S. O. Koswatta, M. S. Lundstrom, and D. E. Nikonov, Nano Lett. **7**, 1160 (2007).
[18] D. Jena *et al.*, Appl. Phys. Lett. **93**, 112106 (2008).
[19] J. Appenzeller *et al.*, Phys. Rev. Lett. **92**, 226802 (2004).
[20] G. Pennington *et al.*, Appl. Phys. Lett. **90**, 062110 (2007).
[21] A. B. Grebene and S. K. Ghandhi, Solid-State Electron. **12**, 573 (1969).
[22] P. K. Ko, in *Advanced MOS Device Physics*, edited by N. G. Einspruch and G. Gildenblat (Academic Press, San Diego, 1989), pp. 1.
[23] L. Marty *et al.*, Phys. Rev. Lett. **96**, 136803 (2006).
[24] The avalanche process was stable and repeatable during all vacuum measurements in this study. The physical breakdown voltage in vacuum appears consistently higher than in air [25] for a given nanotube length, enabling the measurements in Figs. 3 and 4.
[25] E. Pop, Nanotechnology **19**, 295202 (2008).
[26] V. Perebeinos and P. Avouris, Phys. Rev. Lett. **101**, 057401 (2008).